To appear in the International Joint Conference on Biometrics, Washington D.C., October, 2011

3D to 2D Fingerprints: Unrolling and Distortion Correction

Qijun Zhao, Anil Jain*
Department of Computer Science and Engineering
Michigan State University
{qjzhao, jain}@cse.msu.edu

Gil Abramovich
GE Global Research
abramovi@research.ge.com

Abstract

Touchless 3D fingerprint sensors can capture both 3D depth information and albedo images of the finger surface. Compared with 2D fingerprint images acquired by traditional contact-based fingerprint sensors, the 3D fingerprints are generally free from the distortion caused by non-uniform pressure and undesirable motion of the finger. Several unrolling algorithms have been proposed for virtual rolling of 3D fingerprints to obtain 2D equivalent fingerprints, so that they can be matched with the legacy 2D fingerprint databases. However, available unrolling algorithms do not consider the impact of distortion that is typically present in the legacy 2D fingerprint images. In this paper, we conduct a comparative study of representative unrolling algorithms and propose an effective approach to incorporate distortion into the unrolling process. The 3D fingerprint database was acquired by using a 3D fingerprint sensor being developed by the General Electric Global Research. By matching the 2D equivalent fingerprints with the corresponding 2D fingerprints collected with a commercial contact-based fingerprint sensor, we show that the compatibility between the 2D unrolled fingerprints and the traditional contact-based 2D fingerprints is improved after incorporating the distortion into the unrolling process.

1. Introduction

Fingerprints are widely used for personal identification in both forensics and civilian applications. Traditionally, fingerprints have been captured by using an ink-based off-line method or an on-line contact-based (e.g., optical, capacitive, etc.) fingerprint scanner [9]. In either case, the subject has to press (roll) his/her fingers against a surface (e.g., a fingerprint paper card or a glass plate), to obtain 2D fingerprint images. One drawback of these contact-based fingerprint acquisition approaches is that the pressure exerted by the fingers is usually non-uniform and leads to undesirable finger motion (e.g., tracking and torsion) [8, 10]. As a consequence, the captured 2D fingerprint images are often distorted in a nonlinear way. See Fig. 1. Such nonlinear distortion increases the intra-class variations among the fingerprint images of the same finger, and introduces matching errors [12].

(a) (b)

Figure 1. Two 2D plain fingerprint images collected from the same finger by using a contact-based sensor [17]. The image in (b) has torsion and larger distortion than the image in (a). In both images, ridges appear wider in the central part than in the peripheral part.

Touchless fingerprint acquisition technology has been proposed to directly image the fingers without contact between the finger surface and the fingerprint sensor. There are two types of touchless fingerprint technology: 2D images (i.e., texture information only) and 3D images (i.e., texture + depth information). The use of 2D touchless fingerprints has not been as popular as 2D contact-based sensing technology since the curvature of the finger is not taken into account. Here, we primarily focus on 3D touchless fingerprint sensing beacuse of its capability to provide a "rolled equivalent" 2D image that has important implications in law enforcement and homeland security applications. The 3D touchless fingerprint acquisition approach has several advantages since it can capture i) (rolled equivalent) full fingerprints by using multiple cameras (or a single

*Anil Jain is also affiliated with the Department of Brain and Cognitive Engineering, Korea University, Anam-dong, Seongbuk-gu, Seoul 136-713, Korea. His research was partially supported by WCU (World Class University) program funded by the Ministry of Education, Science and Technology through the National Research Foundation of Korea (R31-10008).

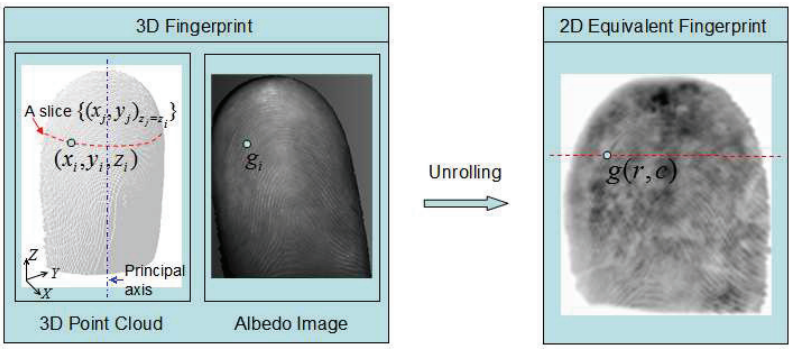

Figure 2. A 3D fingerprint consists of 3D point cloud and the associated albedo image. It can be represented as a set of quaternions $\mathcal{F} = \{(x_i, y_i, z_i, g_i)|i = 1, 2, \cdots, N\}$. Unrolling algorithms convert 3D fingerprints to 2D equivalent fingerprints $F = g(r, c) \in \mathbf{R}^{R \times C}$.

camera with mirrors) [5, 10, 14], ii) both 3D depth information and albedo images of the finger surface [2,6,10,15], and iii) images without the aforementioned distortion caused by non-uniform pressure and undesirable motion of the finger [10].

3D fingerprint images, as a new representation of fingerprints, can not be directly matched with the legacy 2D fingerprints [4]. Further, it is not feasible to replace the 2D fingerprints in existing fingerprint databases with 3D fingerprints. Consequently, any new sensing technology for fingerprints must satisfy the interoperability property due to the lack of existing 3D database and the current lack of 3D fingerprint technology and standards. Of course, in an emerging application where a database of users is being constructed from scratch, the new sensing technology can be used to enroll all the users. Note that since the 3D fingerprint sensors are significantly more expensive than 2D contact-based sensors, we envision that the 3D sensors can be used for acquiring high quality enrollment images and the commodity 2D contact-based sensors can be used for verification.

One approach to address the interoperability issue between 3D fingerprints and traditional 2D fingerprints is to convert the 3D fingerprints to 2D equivalent fingerprints [4]. This conversion is called virtual rolling of 3D fingerprints, and the algorithms for achieving this are called unrolling (or unwrapping) algorithms. While several unrolling algorithms have been proposed in the literature, they do not consider the distortion typically encoutered in capturing 2D fingerprints. To improve the matching accuracy, it is important to take the distortion into consideration when converting 3D fingerprints to 2D equivalent fingerprints.

The objective of this paper is i) to compare the performance of unrolling algorithms proposed in the literature and ii) to propose an effective method for incorporating the distortion into the unrolling process so that the compatibility between the 2D equivalent fingerprints and the traditional 2D fingerprints can be improved. The unrolling algorithms will be evaluated on a set of 3D fingerprints in terms of the compatibility between their obtained 2D equivalent fingerprints and the corresponding traditional 2D fingerprints. Specifically, we will match the 2D equivalent fingerprints against the traditional 2D fingerprints by using a commercial fingerprint matcher, i.e., VeriFinger [1], and compare the matching accuracy on the unrolled 2D fingerprints obtained by different unrolling algorithms. The experimental results show that the 2D equivalent fingerprints and the traditional contact-based 2D fingerprints become more compatible after correcting for distortion.

The rest of this paper is organized as follows. Section 2 briefly reviews published unrolling algorithms. Section 3 introduces the proposed method of distortion-based unrolling. Section 4 presents the experimental results and Section 5 concludes the paper.

2. Related Work

Before we review the unrolling algorithms, we first define the problem of unrolling 3D fingerprints. 3D fingerprints captured by touchless fingerprint sensors consist of two parts: 3D point cloud data and the albedo image. See Fig. 2. Without loss of generality, we denote a 3D fingerprint as a set of quaternions, i.e., $\mathcal{F} = \{(x_i, y_i, z_i, g_i)|i = 1, 2, \cdots, N\}$, where (x_i, y_i, z_i) are the coordinates of the i_{th} point in the fingerprint, g_i is its intensity, and N is the total number of points. We further suppose that the 3D point cloud has been aligned so that the *Z*-axis is along the finger length (i.e., the first principal axis of the finger). Points with the same *z*-coordinate (i.e, at the same length of the finger) consititute a slice (or a cross section) of the finger. Given a 3D fingerprint, an unrolling algorithm maps it to a two dimensional plane and outputs a 2D equivalent fingerprint image, i.e., $F = g(r, c) \in \mathbf{R}^{R \times C}$, where R and C are, repsectively, the numbers of rows and columns in the 2D equivalent fingerprint image, and g is the intensity at the pixel (r, c).

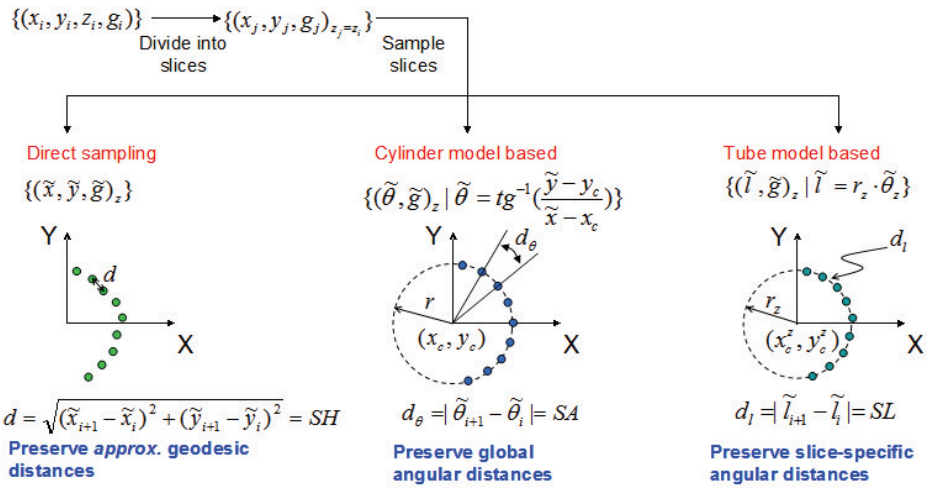

Figure 3. Three representative unrolling algorithms: direct sampling, cylinder model based, and tube model based. They differ from each other in the way they sample slices (the filled-in points denote sampling points in a slice). The cylinder model assumes that all slices are segments of circles that have the same radius; the tube model assumes that all slices are segments of circles, and different slices can have different radii; and the direct sampling method does not assume any model for the finger surface. *SH*, *SA*, and *SL* are the sampling intervals of the three algorithms, respectively.

Available unrolling algorithms can be divided into two categories — parametric and non-parametric — according to whether a model is assumed for the finger surface [4]. Parametric unrolling algorithms assume that the finger surface can be represented as a parametric surface, e.g., cylinder [4], tube [2, 15], and sphere [16]. In the cylinder model, the finger surface is approximated as a cylindrical surface centered at the principal axis of the finger. In other words, the cylinder model assumes that all the slices are segments of circles which have the same radius. The tube model also assumes that all the slices are segments of circles, but their radii (and optionally their center positions) can be different. Unlike parametric methods, non-parametric methods do not assume any models for the finger surfaces. They directly compute the corresponding pixels in the 2D equivalent fingerprint image from the points in the 3D fingerprint.

To unroll a 3D fingerprint, the parametric unrolling algorithms first fit the assumed finger surface model to the point cloud of the 3D fingerprint and estimate the parameters of the model. With the estimated model of the 3D fingerprint, they then generate the 2D equivalent fingerprint by flattening the parametric surface defined by the model. These parametric unrolling methods preserve the angular distances between points in the finger surface, instead of the surface distances between them.

On the contrary, non-parametric unrolling algorithms aim to preserve the geodesic or Euclidean distances between points. In [6] and [13], an iterative algorithm was employed to optimize the locations of the points in the 2D equivalent fingerprint image in the sense that the Euclidean distances between neighboring points in the 3D point cloud are well preserved. In [4], a direct sampling method is proposed. It divides the 3D fingerprint into slices, and chooses a starting point in each slice as the point where the slice and a plane passing through the principal axis of the finger (we call this plane the baseline plane) intersect. In the 2D equivalent fingerprint image, each slice corresponds to a row and the starting points of different slices are in the same column. It then re-samples each slice at equidistance from the starting point towards both ends of the slice, and maps each sampling point to a pixel in the row corresponding to the slice. The direct sampling method in [4] can preserve the geodesic distances between points on the finger surface. Moreover, it allows to choose where to start rolling the fingers, e.g., from left to right or from right to left. As a result, the obtained 2D equivalent fingerprint images can simulate the effect of rolling fingers from "nail to nail", which is required in collecting rolled legacy fingerprint images [11].

To summarize, existing unrolling algorithms can preserve certain distance measurement between points on the finger surface when converting 3D fingerprints to 2D fingerprints. See Fig. 3. However, they do not consider the distortion that is typically present in acquiring traditional contact-based 2D fingerprints [1]. Such distortion can affect the compatibility between the 2D equivalent fingerprints and the traditional 2D fingerprints. Moreover, incorporating nonlinear distortion into unrolling provides more accurate 2D equivalent fingerprints. This not only simplifies distortion

[1] In [16], the authors apply the sphere model to unwrap 3D fingerprints and propose to correct the distortion introduced during the flattening of a spherical surface. But, they did not consider the distortion introduced during the pressing/rolling of the finger that is considered here.

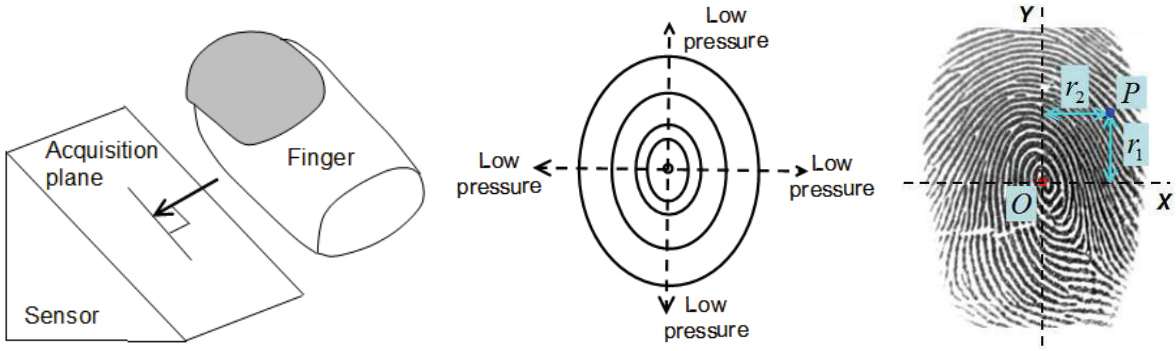

(a) (b) (c)

Figure 4. The proposed distortion model of plain fingerprints. (a) Two assumptions: i) The finger moves towards the sensor along the direction perpendicular to the acquistion plane, and ii) no traction or torsion is applied once the finger gets contacted with the acquistion plane. (b) The pressure decreases from the center to the boundary of the fingerprint. (c) The sampling interval at a point *P* depends on its position with respect to the center *O* (see Equation 1). The farther *P* is from *O*, the larger the sampling interval at *P* is. The fingerprint image is from the FVC2002 database [7].

processing in 2D fingerprint matching, but also makes the matcher more efficient. In the next section, we propose an effective approach to deal with the distortion when converting 3D fingerprints to 2D fingerprints.

3. Distortion-based Unrolling

3.1. Distortion Model

Several different distortion models, such as thin plate spline [3] and average deformation model [12], have been proposed for handling nonlinear distortion in fingerprint matching. These models compute distortion between two fingerprints based on the given corresponding feature points in them. The model presented in [8], on the contrary, simulates nonlinear distortion encountered in a contact-based plain fingerprint; the model has been successfully applied in generating synthetic plain fingerprints. However, the reference non-distorted fingerprint used by the model was defined as the fingerprint which was produced by a correct finger placement, which still suffered from the pressure-induced distortion. As a result, it is not applicable in our case because our reference fingerprints (i.e., the 3D touchless fingerprints) are completely free from the pressure-induced distortion. In the rest of this section, we propose a new distortion model specially designed for unrolling 3D fingerprints.

Plain and rolled fingerprints basically have quite different distortion due to the different ways they are acquired. In this paper, we focus on plain fingerprints. As can be seen from the example plain fingerprints in Fig. 1, ridges usually appear wider in the center than in the periphery of plain fingerprints. One possible reason for this is the non-uniform pressure across the fingerprints: the pressure decreases from the center to the periphery of fingerprints. Because of the plasticity of finger skin, large pressure stretches the skin more than low pressure. Consequently, given an imaging resolution, more points are sampled from the portion where the pressure is large.

The objective of our proposed distortion model is to simulate such non-uniform sampling rates caused by the non-uniform pressure across a plain fingerprint. For simplicity, we make the following two assumptions on plain fingerprint acquisition. i) The finger moves towards the fingerprint sensor along the direction perpendicular to the acquisition plane of the sensor (see Fig. 4(a)). The point on the finger surface which touches the acquisition plane first is defined as the center of the obtained fingerprint (denoted as *O*). ii) No traction or torsion is applied to the finger once it gets in contact with the acquisition plane. Under these assumptions, the pressure reaches the maximum at the center and gradually decreases as we approach the boundary of the fingerprint. See Fig. 4(b). Correspondingly, the sampling interval gradually increases from the center to the boundary.

Taking the center of the fingerprint as the origin, a coordinate system is constructed in the fingerprint: *Y*-axis is along the principal axis of finger and *X*-axis is perpendicular to *Y*-axis. See Fig. 4(c). Let sh_0 be the baseline sampling interval at the center of the fingerprint. Then the sampling interval at a point $P(r_1, r_2)$ is defined as

$$sh = (1 + p \cdot (1 - e^{-r_1^2/k_1} \cdot e^{-r_2^2/k_2})) \cdot sh_0, \qquad (1)$$

where r_1 and r_2 are, respectively, the absolute distances from *P* to the *X*- and *Y*- axes, k_1 and k_2 denote the skin plasticity along the *Y*- and *X*- axes, and *p* represents the amount of pressure. Obviously, the farther *P* is from *O*, the larger the sampling interval at *P* is.

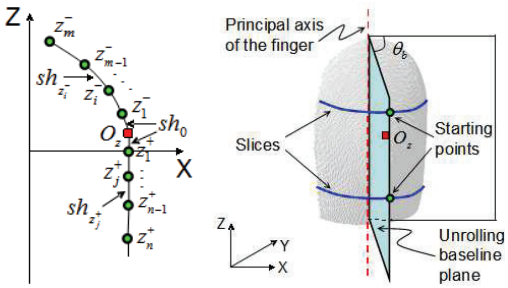

(a) (b)

Figure 5. Illustration of the proposed direct sampling with distortion corrected sampling intervals. (a) The 3D fingerprint is divided into slices along the finger length (i.e., Z-axis) starting from the fingerprint center O_z and using distortion corrected sampling intervals. (b) The sampling starting point on each slice is defined as the intersection point between the slice and a pre-specified unrolling baseline plane.

3.2. The Proposed Unrolling Algorithm

We propose a new unrolling algorithm by incorporating the above-defined adaptive sampling intervals into the direct sampling based unrolling algorithm (denoted as DS). The original DS algorithm [4] uses the same sampling interval for the whole fingerprint, and thus does not cope with the pressure-induced distortion in 2D fingerprints. On the contrary, the unrolling algorithm proposed here adaptively determines a sampling interval for each point in the fingerprint according to its relative position to the center of the fingerprint.

The first step in the proposed algorithm is to divide the 3D point cloud to a set of slices (assume that the point cloud has been aligned so that the *Z*-axis is along the first principal axis of the finger as shown in Fig. 2). In order to compute the sampling interval between slices (i.e., the distance between them along the *Z*-axis), we set the *Z*-axis center as the mean of the *z*-coordinates of all the points in the 3D fingerprint, denoted as O_z. Given the baseline sampling interval sh_0 at the center, the *z*-coordinates of the two slices next to the central slice are $z_1^- = O_z - sh_0$ and $z_1^+ = O_z + sh_0$, respectively. The sampling interval at the slice z_i^- or z_j^+ is then computed as

$$sh_z = (1 + p \cdot (1 - e^{-d^2/k_1})) \cdot sh_0, \qquad (2)$$

where *d* is the absolute difference between the *z*-coordinates of the slice and the central slice. Thus, the *z*-coordinates of the slices next to z_i^- and z_j^+ are, respectively, $z_{i+1}^- = z_i^- - sh_z$ and $z_{j+1}^+ = z_j^+ + sh_z$. With the obtained *z*-coordinates of the slices $\{z_m^-, z_{m-1}^-, \cdots, z_1^-, O_z, z_1^+, \cdots, z_{n-1}^+, z_n^+\}$, we can easily divide the 3D point cloud into $(m + n + 1)$ slices. See Fig. 5(a)

In the second step, each slice is further sampled. The sampling starting point on each slice is defined as the intersection point between the slice and a pre-specified unrolling baseline plane (see Fig. 5(b)). The baseline plane passes the principal axis of the finger and composes an angle of θ_b with the *X*-*Z* plane. Let $O_i(x_i^0, y_i^0, z_i)$ be the starting point on the slice z_i. The sampling interval at a point $P(x_i^k, y_i^k, z_i)$ on this slice is calculated as follows,

$$sh_{z_i}^k = (1 + p \cdot (1 - e^{-d_z^2/k_1} \cdot e^{-d_s^2/k_2})) \cdot sh_0, \qquad (3)$$

where $d_z = |z_i - O_z|$ and d_s is the geodesic distance between *P* and O_i along the slice. Starting from O_i, the slice is then sampled towards both ends according to the calculated sampling interval.

In the last step, a 2D equivalent fingerprint image *F* is obtained based on the sampling points: each slice is a row in *F*, and each sampling point on each slice is a pixel on the slice's corresponding row in *F*, while the starting points correspond to the central column in *F*.

4. Experimental Results

4.1. Database

The fingerprint database used in this paper includes a set of frontal-view 3D fingerprints and their corresponding 2D plain fingerprints. The 3D fingerprints were captured by using a 3D fingerprint sensor being developed by the General Electric Global Research, while the corresponding 2D plain fingerprints were captured with a commercial contact-based fingerprint sensor. Totally, we have collected data from 24 fingers with one 3D fingerprint and one plain fingerprint for each of the fingers. The collected 3D fingerprint data has varying precision in depth information. Twenty of the 3D fingerprints have very noisy depth information. They are used to evaluate the robustness of different unrolling algorithms. The other four fingerprints have more precise depth information, and are used to evaluate the compatibility of unrolled 2D equivalent fingerprints and 2D contact-based plain fingerprints.

4.2. Comparison between Unrolling Algorithms

We first compared the three representative unrolling algorithms depicted in Fig. 3 (namely, cylinder model based (CYL), tube model based (TUBE), and direct sampling (DS)) using the twenty noisy 3D fingerprints. We observed that when the depth information of 3D fingerprints is very noisy, the CYL and TUBE algorithms do not perform well. This is because both CYL and TUBE assume that slices of 3D fingerprints are segments of circles. However, such an assumption might be violated in noisy 3D fingerprints. In other words, erroneous circles could be fitted to the slices of noisy 3D fingerprints (see Fig. 6). Consequently, CYL and TUBE models can not correctly unroll the 3D fingerprints or generate the 2D equivalent fingerprints. While the DS

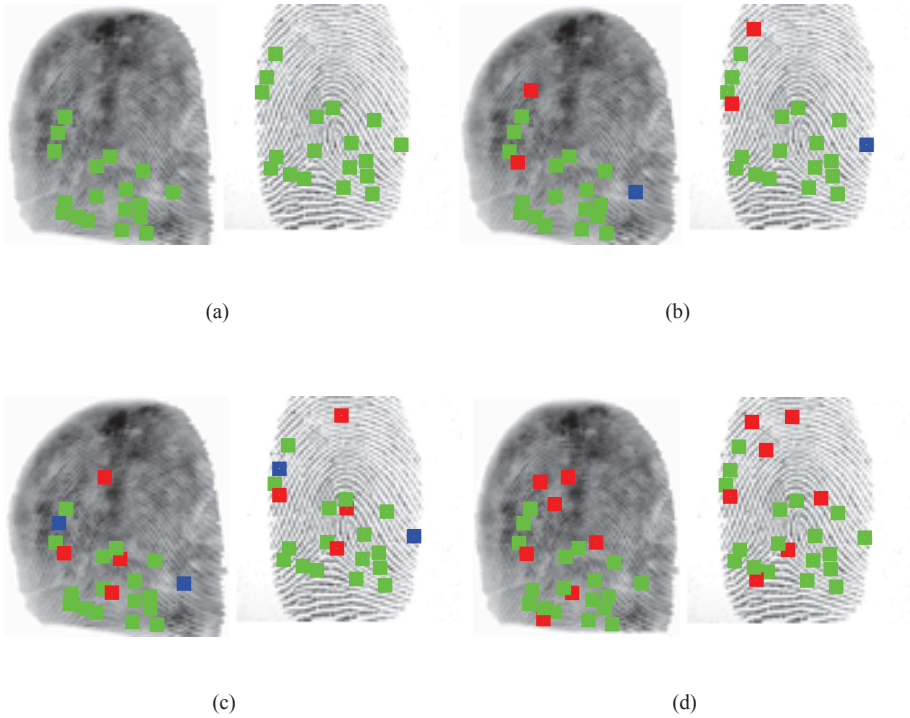

(a) (b) (c) (d)

Figure 7. The mated minutiae in the 2D equivalent fingerprint images of an example 3D fingerprint obtained by using the (a) cylinder model based (CYL), (b) tube model based (TUBE), (c) direct sampling (DS), and (d) proposed direct sampling with distortion correction (DSwDC) algorithms. The results of CYL in (a) are taken as baseline, and the mated minutiae are shown in green color. The red minutiae in (b)-(d) are the mated minutiae found by the other algorithms, but not by CYL. The blue minutiae in (b)-(c) are the mated minutiae found by CYL, but missed by the other algorithms.

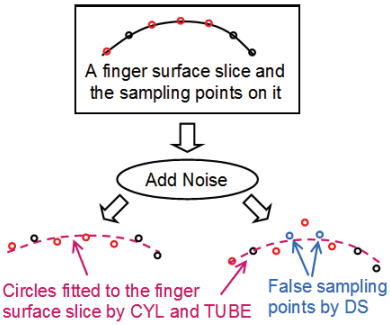

Figure 6. Sensitivity of unrolling algorithms to depth errors. Depth errors can lead to incorrect radii of the circles fitted by CYL and TUBE models, and hence inaccurate sampling points. DS can also sample false points due to depth errors.

algorithm also generates false sampling points due to depth errors (see Fig. 6), as we will show later, DS generally performs better in unrolling 3D fingerprints with precise depth information. Therefore, we incorporate the proposed distortion correction technique into the DS algorithm. Next, we report the experimental results of CYL, TUBE, DS, and the proposed direct sampling with distortion correction (DSwDC) algorithm on four 3D fingerprints for which precise depth information is available.

We use CYL as the baseline. In [13], the performance of unrolling algorithms was evaluated by the quality of the obtained 2D equivalent fingerprint images of three example 3D fingerprints. In this paper, on the contrary, we compare different unrolling algorithms according to the accuracy of matching their generated 2D equivalent fingerprints and the corresponding contact-based 2D plain fingerprints, because this is a more direct way to assess the compatibility between the obtained 2D equivalent fingerprints and the traditional contact-based fingerprints. The fingerprint matching in our experiments is done by using a commercial fingerprint matcher, called VeriFinger [1].

Figure 7 shows the 2D equivalent fingerprint images [2] of an example 3D fingerprint and the mated minutiae found by VeriFinger between them and the corresponding contact-based 2D plain fingerprint. Note that the 2D equivalent

[2] Please note that we intentionally blur the fingerprint images and show only the minutia locations because of the privacy protection constraint of this project.

Method	CYL	TUBE	DS	DSwDC
# Mated Minutiae	12	13	14	17

Table 1. The average number of mated minutiae in the 2D equivalent fingerprints generated by the CYL, TUBE, DS, and proposed DSwDC algorithms.

fingerprint images have been post-processed by applying adaptive histogram equivalization to improve the contrast, and the pixel values are reversed to make the ridge pixels dark and the valley pixels bright so that they are consistent with traditional contact-based fingerprints in which valleys are brighter than ridges. From these results, it can be seen that the CYL algorithm tends to over-sample the top portion of the fingerprint because it uses the same radius for all the slices across the fingerprint. As a result, the image generated by CYL obtains the minimum number of mated minutiae (i.e., 18). The results of the TUBE and DS algorithms are very similar. The numbers of mated minutiae in the images generated by TUBE and DS are, respectively, 19 and 20. The largest number of mated minutiae (i.e. 25) are obtained in the 2D equivalent fingerprint image generated by the proposed DSwDC algorithm.

4.3. Effectiveness of Distortion Correction

Figure 8 shows the matching results in a portion of the 2D equivalent fingerprints of an example 3D fingerprint. Mated minutiae in the 2D equivalent fingerprint generated by the baseline CYL algorithm are shown in green color; the mated minutiae found by the other algorithms but not by CYL are marked by red color; and the mated minutiae missed by the other algorithms are displayed in blue color. Table 1 gives the average number of mated minutiae in the 2D equivalent fingerprints generated by the four algorithms. Obviously, many more minutiae in the DSwDC generated 2D equivalent fingerprint image can be matched with the minutiae in the contact-based 2D plain fingerprint.

The relatively poor matching accuracy of the 2D equivalent fingerprints generated by the other unrolling algorithms is due to the fact that minutiae matching is dependent on the spatial configuration of minutiae, which is easily affected by fingerprint distortion. By simulating the pressure-induced distortion in 2D plain fingerprints, the proposed DSwDC unrolling algorithm achieves better matching accuracy. This demonstrates the effectiveness of distortion correction in improving the compatibility between 2D equivalent fingerprints and traditional contact-based fingerprints.

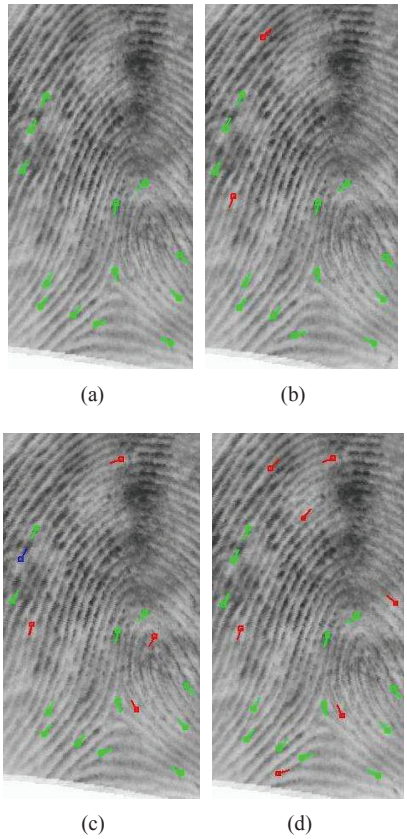

Figure 8. The mated minutiae in a portion of the 2D equivalent fingerprints of an example 3D fingerprint obtained by using the (a) CYL, (b) TUBE, (c) DS, and (d) proposed DSwDC algorithms.

5. Conclusions

In this paper, we studied the impact of fingerprint distortion on the compatibility of traditional contact-based fingerprints and 2D equivalent fingerprints obtained by unrolling 3D fingerprints. By analyzing the pressure exerted by the finger in acquiring contact-based plain fingerprints, we proposed a distortion model to adaptively determine the sampling intervals across fingerprints. Further, we presented a novel approach to unrolling 3D fingerprints based on the distortion corrected sampling intervals. The experimental results on several available 3D fingerprints and their corresponding contact-based plain fingerprints demonstrated that the compatibility between the 2D equivalent fingerprints and traditional contact-based plain fingerprints can be effectively improved by incorporating distortion into the unrolling process. In our ongoing work, we are studying the sensitivity of the parameters involved in the unrolling algorithm and improving the compatibility between 2D rolled equivalent fingerprints and legacy rolled fingerprints by investigating the distortion in rolled fingerprints. As the sensor is still in the prototype stage, we expect to provide our distortion correction results to sensor designers to further improve the sensor characteristics and collect additional data.

Aknowledgment

This research was conducted at Michigan State University and GE Global Research and was funded by the Science and Technology Directorate of the U.S. Department of Homeland Security under contract HSHQDC-10-C-00083. We would like to thank Christopher Nafis and Mehdi Daneshpanah for their support in processing and providing fingerprint input data, and in providing insights in the 3D capture algorithms.

References

[1] Neurotechnology Inc., VeriFinger. `http://www.neurotechnology.com`.

[2] G. Abramovich, K. Harding, S. Manickam, J. Czechowski, V. Paruchuru, R. Tait, C. Nafis, and A. Vemury. Mobile, Contactless, Single Shot, Fingerprint Capture System. In *Proc. SPIE*, volume 7667, 2010.

[3] A. M. Bazen and S. Gerez. Fingerprint Matching by Thin-Plate Spline Modeling of Elastic Deformations. *Pattern Recognition*, 36(8):1859–1867, 2003.

[4] Y. Chen, G. Parziale, E. Diaz-Santana, and A. K. Jain. 3D Touchless Fingerprints: Compatibility with Legacy Rolled Images. In *Proc. Biometric Symposium*, 2006.

[5] H.-S. Choi, K. Choi, and J. Kim. Mosaicing Touchless and Mirror-Reflected Fingerprint Images. *IEEE Transactions on Information Forensics and Security*, 5(1):52–61, 2010.

[6] A. Fatehpuria, D. L. Lau, and L. G. Hassebrook. Acquiring a 2D Rolled Equivalent Fingerprint Image from a Non-Contact 3D Finger Scan. In *Proc. SPIE*, 2006.

[7] D. Maio, D. Maltoni, R. Cappelli, J. L. Wayman, and A. K. Jain. The Second International Competition for Fingerprint Verification Algorithms (FVC2002), April, 2002. `http://bias.csr.unibo.it/fvc2002/`.

[8] D. Maltoni and R. Cappelli. Advances in Fingerprint Modeling. *Image and Vision Computing*, 27:258–268, 2009.

[9] D. Maltoni, D. Maio, A. K. Jain, and S. Prabhakar. *Handbook of Fingerprint Recognition (Second Edition)*. Springer-Verlag, 2009.

[10] G. Parziale. Touchless Fingerprint Technology. In N. K. Ratha and V. Govindaraju, editors, *Advances in Biometrics: Sensors, Algorithms and Systems*, chapter 2, pages 25–48. Springer, 2008.

[11] G. Parziale and Y. Chen. Advanced Technologies for Touchless Fingerprint Recognition. In M. Tistarelli, S. Z. Li, and R. Chellappa, editors, *Handbook of Remote Biometrics*, chapter 4, pages 83–109. Springer, 2009.

[12] A. Ross, S. C. Dass, and A. K. Jain. Fingerprint Warping Using Ridge Curve Correspondences. *IEEE Transactions on Pattern Analysis and Machine Intelligence*, 28(1):19–30, 2006.

[13] S. Shafaei, T. Inanc, and L. G. Hassebrook. A New Approach to Unwrap a 3D Fingerprint to a 2D Rolled Equivalent Fingerprint. In *Proc. BTAS*, 2009.

[14] L. A. Sweeney, V. W. Weedn, and R. Gross. Method and System for Capturing Fingerprints, Palm Prints, and Hand Geometry. US Patent No. 7660442B2, Feb. 9, 2010.

[15] Y. Wang, L. G. Hassebrook, and D. L. Lau. Data Acquisition and Processing of 3D Fingerprints. *IEEE Transactions on Information Forensics and Security*, 5(4):750–760, 2010.

[16] Y. Wang, D. L. Lau, and L. G. Hassebrook. Fit-Sphere Unwrapping and Performance Analysis of 3D Fingerprints. *Applied Optics*, 49(4):592–600, 2010.

[17] C. I. Watson. NIST Special Database 24 Digital Video of Live-Scan Fingerprint Data, July. 27, 1998. `http://www.nist.gov/srd/nistsd24.cfm`.